JOURNAL OF PROPULSION AND POWER
Vol. 17, No. 1, January–February 2001

Velocity and Temperature Statistics in Reacting Droplet-Laden Homogeneous Shear Turbulence

Farzad Mashayek*
University of Hawaii at Manoa, Honolulu, Hawaii 96822

The results of numerical simulations are used to investigate the effects of the mass-loading ratio and the droplet time constant on the velocity and temperature statistics in a two-phase homogeneous shear turbulence. The fuel vapor generated by the evaporation of the droplets reacts with the oxidizer carrier gas through a single-step, second-order reaction. The carrier phase is simulated in the Eulerian frame using direct numerical simulation, whereas the droplets are tracked in a Lagrangian manner. It is shown that the turbulence kinetic energy and its small-scale viscous dissipation rate increase with the decrease of either the mass-loading ratio or the droplet time constant. The opposite trend is observed for the early variations of the extra dissipation, which results from the drag. It appears that the velocity and temperature fluctuations of the dispersed phase can be reasonably described by Gaussian distribution. The increase of the mass loading ratio increases both the mean temperature of the carrier phase and the Lagrangian mean temperature difference between the phases. The increase of the droplet time constant however decreases the former while increasing the latter.

Nomenclature

B	=	$(T^* - T_d)/\Lambda$ transfer number
C_p, C_v	=	specific heats of the carrier phase
D_d	=	contribution of the drag to turbulence kinetic energy
d_d	=	droplet diameter
f_1	=	$(1 + 0.15Re_d^{0.687})/(1 + B)$
h_p^f	=	enthalpy of formation of the product gas
K_{fwd}	=	forward reaction rate constant
k	=	$\langle \rho u_i u_i \rangle/2$ carrier-phase turbulence kinetic energy
k_d	=	$\langle\langle v_i v_i \rangle\rangle/2$ dispersed-phase turbulence kinetic energy
L_f	=	reference length
L_v	=	latent heat of vaporization of the liquid
M	=	$(u_i u_i/\gamma RT)^{1/2}$ turbulence Mach number
m_d	=	mass of the droplet
N_d	=	total number of droplets for each simulation
n_d	=	number of droplets within the cell volume
R	=	gas constant
r	=	stoichiometric coefficient
S	=	$\partial\langle U_1 \rangle/\partial x_2$ mean velocity gradient
T	=	temperature
t	=	time
U_f	=	reference velocity
U_i	=	instantaneous velocity of the carrier phase
u_i	=	fluctuating velocity of the carrier phase in direction x_i $(i = 1, 2, 3)$
v_i	=	fluctuating velocity of the droplet in direction x_i
x_i	=	spatial coordinates
Γ	=	binary mass diffusivity coefficient
γ	=	ratio of the specific heats of the carrier gas
Δ	=	$\partial u_j/\partial x_j$ dilatation
δ_{ij}	=	Kronecker delta function
$\delta\mathcal{V}$	=	cell volume
ϵ	=	viscous dissipation rate
η	=	Kolmogorov length scale
κ	=	thermal conductivity of the carrier phase
μ	=	viscosity of the carrier phase
ρ	=	density
ω_i	=	vorticity component
$\langle\ \rangle$	=	Eulerian ensemble average over the number of collocation points
$\langle\langle\ \rangle\rangle$	=	Lagrangian ensemble average over the number of droplets

Subscripts

b	=	base case
d	=	droplet properties
f	=	reference parameters for normalization
rms	=	root mean square
0	=	initial value (at $t = 0$)

Superscript

$*$	=	carrier phase properties at the droplet location

Received 26 August 1999; presented as Paper 2000-0183 at the AIAA 38th Aerospace Sciences Meeting and Exhibit, Reno, NV, 10–13 January 2000; revision received 7 February 2000; accepted for publication 13 April 2000.

*Assistant Professor, Department of Mechanical Engineering, 2540 Dole Street; currently Associate Professor, Department of Mechanical Engineering, University of Illinois at Chicago, 842 West Taylor Street, 2053 ERF, Chicago, Illinois 60607; mashayek@uic.edu. Senior Member AIAA.

Introduction

ACCURATE description of dispersion of solid particles and liquid droplets in turbulent flows imposes many challenges from an analytical point of view. This is mainly considered a result of the numerous degrees of freedom associated with turbulent flows, which inevitably demands a very large computational effort. Despite a significant increase in the computational power in recent years, it seems unlikely that, at least for a foreseeable future, turbulent flows of practical interest can be simulated in an exact manner such as direct numerical simulation (DNS). Therefore, modeling is needed to decrease the number of degrees of freedom such that they can be resolved numerically with a (preferably) much less effort. The models are generally derived following a long and complex mathematical procedure, subject to simplifying assumptions; thus, they must be assessed against more accurate data. Laboratory measurements can be used to generate the data for model validation; however, they are mostly limited to somewhat global and average flow variables.

An alternative can be provided by DNS data of simple (homogeneous) flows whose simulation is feasible with the available computational resources. Although these simple flows do not exhibit all of the complexities involved in practical situations, they can be considered as basic flows locally prevailing in more general inhomogeneous configurations. Consequently, model validation in these flows can be considered as a logical first step. Although establishing a good agreement between the model and the data in these flows does not, necessarily, guarantee acceptable performance in more complex flows, the reverse may be true. That is, if a model fails when compared against basic flows, there is little chance of success

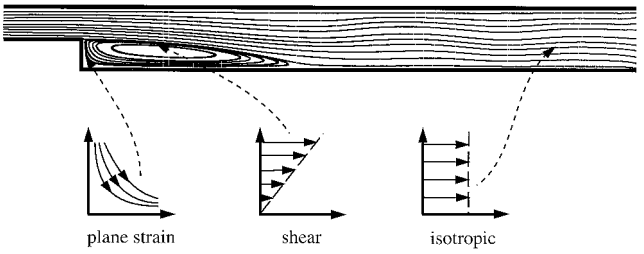

Fig. 1 Correspondence between simple homogeneous flows and various regions in a backward-facing step flow.

in a flow of practical interest. As an example, the schematic in Fig. 1 shows the correspondence between three basic flows and various regions in a backward-facing step flow, which could be used as a good model for many applications including a dump combustor. The basic flows shown in the figure include homogeneous isotropic, homogeneous shear, and homogeneous plane-strain flows, which have been recently studied by DNS and large-eddy simulation in both single- and two-phase systems. A relatively rich database is now available for most of these flows, and they have already been implemented by various investigators to validate turbulence models at different stages.[1–3] The validation process involves comparisons for various Reynolds stresses, dispersion functions, and correlations between the temperature and other flow variables. The DNS results have also been very helpful in providing the much-needed physical insight during the early stages of model development. This valuable opportunity offered by DNS provides a direct means for the assessment of basic modeling assumptions, which mostly stem from theoretical analysis of isotropic and homogeneous flows. The form of the energy spectrum, the behavior at dissipation scales, and the autocorrelation of the fluctuating velocity of the fluid particle as seen by the solid particle are only a few examples.

A review of the existing literature[4] clearly indicates that the extent of DNS studies addressing dispersion of liquid droplets in a compressible flow is very limited. Recently, we presented[4] simulations of liquid droplets dispersed in a homogeneous shear turbulent flow in the presence of evaporation and chemical reaction. The simulations were used to study the evolution of the oxidizer, the fuel vapor, and the droplet-size distribution. The results indicated that the droplets are mainly aligned in the direction of the mean flow, in agreement with a recent theory by Hyland et al.[3] for dispersion of solid particles in an incompressible carrier phase. Further, it was shown that the reaction is much more intense in the regions with high droplet concentration. Consequently, the reaction zone is strongly affected by large-scale mean shear as well as small-scale preferential distribution[5,6] of the droplets in high strain rate regions of the flow.

In this work we use the same simulations to analyze the statistics of the velocity and temperature, which were not discussed in Mashayek.[4] In recent years a wide variety of configurations have been considered by various investigators to study two-phase turbulent flows, including homogeneous isotropic,[7–9] homogeneous anisotropic,[10–12] and inhomogeneous.[13–16] Among these, the homogeneous shear flow (where the magnitudes of the normal Reynolds stresses differ in various directions) provides a very convenient framework for the study of anisotropy effects. An attractive feature of this flow is the possibility of calculating statistics using the entire flowfield. This is made possible in our study by solving all of the governing equations in a deforming coordinate, which renders both phases homogeneous. Another useful feature offered by this flow is its transient nature, which allows the presentation of the time-dependent statistics. These features make the statistics generated by simulations of homogeneous shear flow very valuable for model validation.[1,10] In the following section we provide a brief description of the formulation and methodology. The governing equations and more details can be found in Mashayek.[4,11]

Formulation and Methodology

We consider the motion of a large number of evaporating fuel droplets in an oxidizer carrier gas. It is assumed that the fuel vapor and the oxidizer participate in the single-step, second-order irreversible reaction:

$$\boldsymbol{F} + r\boldsymbol{O} \xrightarrow{K_{\text{fwd}}} (1+r)\boldsymbol{P} \tag{1}$$

where $\boldsymbol{F}$, $\boldsymbol{O}$, and $\boldsymbol{P}$ refer to the fuel vapor, the oxidizer, and the product, respectively. To study the anisotropy features, a homogeneous shear flow is considered, which is characterized by a linear mean velocity profile (see Fig. 1) such that the carrier-phase instantaneous velocity is expressed as $U_i = Sx_2\delta_{i1} + u_i$, where $S = \partial\langle U_1\rangle/\partial x_2 = \text{const}$. Here, $i = 1, 2, 3$ refers to streamwise, cross-stream, and spanwise directions, respectively. Unless stated otherwise, throughout this paper the mean and fluctuating variables are calculated by (density-weighted) Favre averaging.

To increase the computational efficiency and the accuracy of the simulations, a Fourier pseudospectral method is used. This is accomplished by solving the governing equations for fluctuating velocities on a grid, which deforms with the mean flow such that periodic boundary conditions can be imposed. The droplet equations are also solved in the moving coordinate, which allows us to implement periodic boundary conditions, i.e., when a droplet leaves the computational domain from one side, it is substituted by another droplet with the same conditions at the opposite side of the domain. In this manner the total number of the droplets is kept the same for the entire simulation, except for the very small droplets that are removed as a result of other considerations as discussed in the next section. The details of the coordinate transformation and all of the governing equations are given in Ref. 4. These include the compressible forms of the continuity, momentum, and energy equations for the continuous phase coupled with the Lagrangian equations for droplets position, velocity, temperature, and mass. Further, conservation equations (in the Eulerian frame) are considered for mass fractions of the fuel vapor and the oxidizer. The fuel vapor and the product are assumed to have the same molecular weight, viscosity, mass diffusivity, and specific heat as those of the oxidizer gas, such that the mixture of the gas, the fuel vapor, and the product can be treated as one fluid, referred to as the carrier phase.

The carrier phase is considered to be a compressible and Newtonian fluid with zero bulk viscosity and to obey the perfect-gas equation of state. The carrier-phase energy equation is solved for the summation of the sensible internal energy ($\rho C_v T$) and the turbulence kinetic energy ($\frac{1}{2}\rho u_i u_i$) of the oxidizer-vapor-product mixture. This equation is derived by assuming unity Lewis number[17] ($Le \equiv Sc/Pr = 1$). The evaporating droplets remain spherical with diameters smaller than the smallest length scale of the turbulence. The density of the liquid is considered to be constant and much larger than the density of the carrier gas such that only inertia and (modified Stokesian) drag forces are significant to the droplet dynamics. In addition, the volume fraction of the dispersed phase is assumed to be small and both droplet-droplet interactions and heat transfer caused by radiation are neglected. Various empirical correlations are implemented to account for convective effects and modifications caused by a large-droplet Reynolds number in the calculation of momentum, mass, and heat transfer between the phases.[4] The vapor mass fraction at the surface of the droplet is proportional to the partial pressure of the vapor and is described through the Clausius–Clapeyron relation. The integrated effects of the droplets on the carrier phase are accounted for by introducing source/sink terms in the Eulerian equations. These Eulerian terms are calculated from the droplet Lagrangian variables by volume averaging the contributions from all of the individual droplets residing within the cell volume centered around each grid point.[18] All of the variables are normalized by reference length, density, velocity, and temperature scales. A listing of the nondimensional parameters that appear in the formulation is given here: $Ce = [1/(\gamma-1)M_f^2][\Lambda - (1+r)(h_p^f/C_pT_f)]$, heat-release coefficient; $Da = \rho_f L_f K_{\text{fwd}}/U_f$, Damköhler number; $M_f = U_f/\sqrt{(\gamma RT_f)}$, reference Mach number; $Pr = C_p\mu/\kappa$, Prandtl number; $Re_f = \rho_f U_f L_f/\mu$, reference Reynolds number; $Sc = \mu/\rho\Gamma$, Schmidt number; $\Lambda = L_v/C_pT_f$, normalized latent heat of evaporation; $\tau_d = Re_f\rho_d d_d^2/18$, droplet time constant; and Φ_m = droplet mass/gas mass, mass-loading ratio.

The computational methodology and the initialization are also explained in Ref. 4 and will not be detailed here. All of the Eulerian fields are calculated using a pseudospectral method, and the droplet Lagrangian equations are integrated using a second-order-accurate Adams–Bashforth method. To evaluate the carrier phase variables at the droplet location, a fourth-order-accurate Lagrange polynomial interpolation scheme is employed. The density and velocity fields are initialized as random Gaussian, isotropic, and solenoidal fields in Fourier space. The initial temperature field has no fluctuations, and the initial pressure field is calculated using the equation of state. The droplets are initially distributed randomly in the flow with a uniform size and the same velocity and temperature as those of their surrounding fluid. The initial mean-gas density and mean-gas temperature are used as the reference scales for density and temperature, respectively. We choose $M_f = 1$ so that the speed of sound based on the initial mean-gas temperature is the reference scale for the velocity.

Results

All of the simulations are performed on 96^3 collocation points, using as many as 1.24×10^6 droplets (see Table 1), and are continued until the nondimensional time $St = 14$. Although a wide variety of cases have been considered,[4] because of space limitations, here we only discuss the effects of the mass-loading ratio and the droplet time constant on velocity and temperature fields. A listing of the simulations considered in this study is provided in Table 1. Here, we consider a base case, indicated by boldface in the table, and then change the value of one of the parameters in each of the following simulations. For all of the cases, $Re_f = 500$, $Pr = Sc = 0.7$, $\gamma = 1.4$, $S = 2$, $\rho_d = 500$, $\Lambda = 0.8$, $Da = 0.5$, $Ce = 20$, and $r = 1$. The results of the reacting simulations are compared (wherever possible) with the data from a one-way coupling case. The abbreviation used to refer to each case in the presentation of the results is shown in the first column of Table 1. The droplets begin to evaporate and react at the normalized time $St = 2$ when the carrier-phase turbulence kinetic energy starts to grow (see Fig. 2a). The condition of one- or two-way coupling, however, is imposed from $t = 0$ for corresponding cases. To avoid very small droplets, a criterion was set in the code to remove the droplets when $d_d < \sim 0.1\eta$. Only for the case with $\tau_{d0} = 0.5\tau_{d0b}$ did the application of this criterion result in the removal of some of the droplets for $St \geq 12$. This has affected some of the statistics pertaining to this case (for $St \geq 12$) as can be seen in Figs. 2a and 2b.

The temporal variation of the turbulence kinetic energy of the carrier phase $k = \frac{1}{2}\langle \rho u_i u_i \rangle$ is shown in Fig. 2a. For all of the cases, there is an initial ($St < 2$) decay of the kinetic energy because of the isotropic initial velocity field, which lacks the shear Reynolds-stress component and sets the production term in the transport equation for k (see Ref. 11) equal to zero. Once the shear-stress component is generated by the imposed mean velocity gradient the homogeneous shear flow is established, and the kinetic energy starts to grow, approximately at $St = 2$. This time is chosen for initiating the evaporation and reaction. Our previous results[11] show that the presence of the droplets (without evaporation and reaction) decreases the turbulence level by introducing an extra dissipation [see Eq. (3)]. This is in agreement with early variations of the kinetic energy in Fig. 2a. At long times, however, an increase in k is observed in reacting cases as compared to the one-way coupling case. As pointed out by Mashayek,[11] there are two mechanisms involved in this increase of the turbulence level: 1) the decrease of the size of the droplets, which decreases the drag dissipation, and 2) the transfer of the kinetic energy from the dispersed phase to the carrier phase by the evaporated mass. To assess the contribution made by the evaporated mass to the changes of the turbulence kinetic energy, in Fig. 2b, we consider the temporal variations of half of the carrier phase velocity variance $\frac{1}{2}\langle u_i u_i \rangle$. The difference between the curves for similar cases in Figs. 2a and 2b is a quantitative measure of the effects of changes in ρ on the kinetic energy. We also note from Fig. 2a that the decrease of either the mass-loading ratio or the droplet time constant results in the increase of the turbulence kinetic energy at all times.

Table 1 Cases considered in the study

Case reference	Coupling	Evaporation	Reaction	Φ_{m0}	τ_{d0}	$N_d \times 10^{-5}$
One-way	1-way	No	No	——	1.0	1.55
Base case	**2-way**	**Yes**	**Yes**	**0.2**	**1.0**	**3.10**
$2\Phi_{m0b}$	2-way	Yes	Yes	0.4	1.0	6.20
$4\Phi_{m0b}$	2-way	Yes	Yes	0.8	1.0	12.40
$0.5\tau_{d0b}$	2-way	Yes	Yes	0.2	0.5	8.77

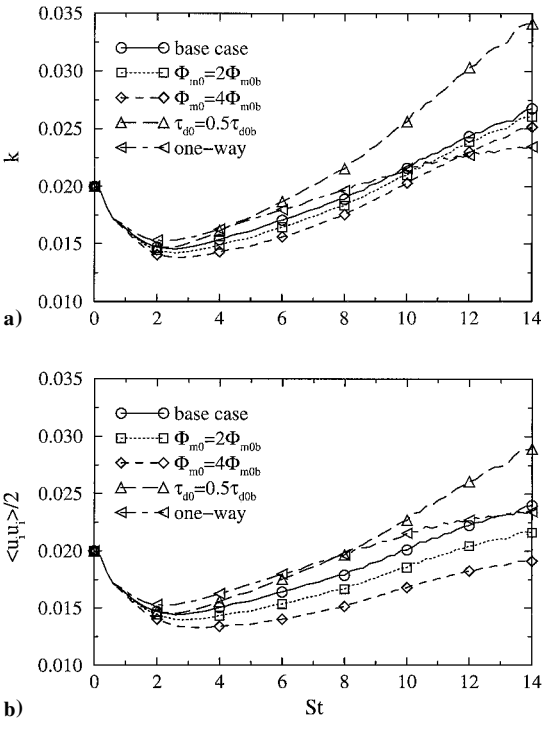

Fig. 2 Temporal variations of a) the turbulence kinetic energy and b) the velocity variance of the carrier phase.

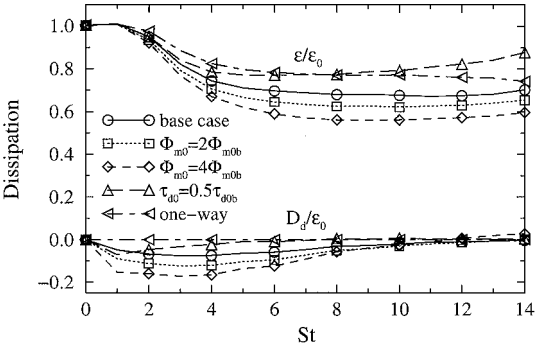

Fig. 3 Temporal variations of the dissipation rate ϵ of the carrier phase. Also shown on the figure is the variation of the drag contribution D_d to the carrier-phase turbulence kinetic energy. Both of the parameters are normalized with the initial value of the dissipation rate ϵ_0.

More insight into the evolution of the turbulence kinetic energy is gained by examining the variations of the (viscous) dissipation rate:

$$\epsilon = (1/Re_f)\left(\langle \omega_i \omega_i \rangle + \tfrac{4}{3}\langle \Delta^2 \rangle\right) \tag{2}$$

The temporal evolution of ϵ, normalized with its initial value (ϵ_0), is shown in Fig. 3. In the case of solid particles interacting with turbulence, the two-way coupling tends to decrease the dissipation rate because of a decrease in the velocity fluctuations.[11] However, in the presence of evaporation and reaction the decrease in the total dissipation rate is less pronounced. This is more noticeable in the case with smaller initial droplet time constant, which results in ϵ

values larger than those in the one-way coupling case toward the end of the simulation. This is caused by the increase of the turbulence level in this case as noted in Fig. 2b. Also shown in Fig. 3 is the temporal variation of

$$D_d = -\left\langle \frac{1}{\delta\mathcal{V}} \sum^{n_d} \left[\frac{f_1 m_d}{\tau_d} \left(u_i^* - v_i\right) u_i^* \right] \right\rangle \tag{3}$$

which represents the contribution of the droplets drag to the variation of the turbulence kinetic energy. A negative value for D_d indicates a decrease of the turbulence kinetic energy by drag. Figure 3 shows that the magnitude of D_d increases during the early stages as the droplets, because of their inertia, cannot follow the rapid changes in the carrier phase and the relative velocity between the two phases increases. At longer times the influence of the initial conditions vanishes, and $|D_d|$ starts to decrease toward small values. For the case with $\Phi_{m0} = 4\Phi_{m0b}$, D_d assumes positive values toward the end of the simulation, which indicates an energy transfer from the droplets to the carrier phase. Previous studies[19,20] show that, in the presence of a mean velocity gradient, the droplet velocity fluctuations in the streamwise direction can exceed those of the fluid. This explains the positive values of D_d at the end of the simulation. The negative values, observed for most of the simulation time, are caused mainly by the misalignment of the fluid and droplet velocity fluctuations as discussed in Fig. 4.

One of the most important features of homogeneous shear flow is the anisotropy of the normal Reynolds-stress components, which makes this flow very valuable for the assessment of various Reynolds-stress models.[1,2] In the assessment the results of the simulations at an early time are taken as the initial conditions, and the prediction of the models for Reynolds stresses are compared with those from the simulations at longer times. The anisotropy of the dispersed phase can be demonstrated by considering the differences between the normalized Reynolds stresses in various directions as shown in Fig. 5. In the figure $k_d = \frac{1}{2}\langle\langle v_i v_i\rangle\rangle$ is the turbulence kinetic energy of the dispersed phase, and no summation is assumed on Greek indices. A comparison with the Reynolds-stress components of the carrier phase (not shown) indicated that the dispersed phase is more anisotropic than the carrier phase. With the neglect of the droplet-droplet interaction, there is no direct mechanism similar to the fluid pressure (within the dispersed phase) for the exchange of energy among various directions. This significantly enhances the differences between the Reynolds-stress components in the dispersed phase during the early stages of the simulations. At longer times the indirect effects of the fluid pressure on the droplets (through drag) diminish the level of anisotropy in the dispersed phase. The results in Fig. 5 indicate that the anisotropy of the dispersed phase decreases with the decrease of either the mass-loading ratio or the droplet time constant. With the decrease of the droplet time constant, the dispersed phase behaves more closely to the carrier phase, which is generally less anisotropic because of the influence of the pressure. On the other hand, the increase of the mass-loading ratio diminishes the overall influence of the carrier phase on the droplets, and so the fluid is less effective in reducing the anisotropy of the dispersed phase.

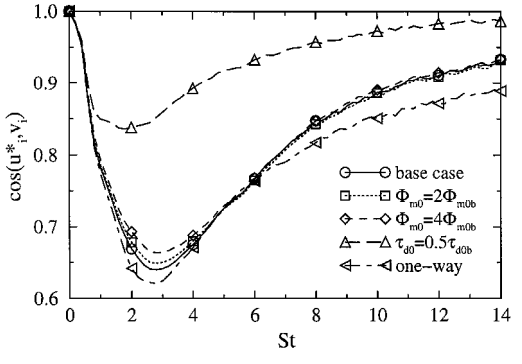

Fig. 4 Alignment of the velocity of the droplets with the velocity of the carrier phase.

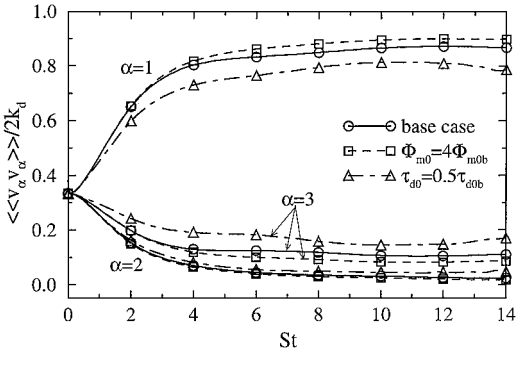

Fig. 5 Anisotropy of the dispersed phase.

The effects of evaporation and reaction on the alignment of the droplet velocity with the carrier-phase velocity can be investigated by considering the temporal evolution of $\cos(u_i^*, v_i) = \langle\langle u_i^* v_i\rangle\rangle / [\langle\langle (u_i^*)^2\rangle\rangle \langle\langle v_i^2\rangle\rangle]^{1/2}$. This alignment affects the magnitude of the correlation between the droplet and fluid velocities $\langle\langle u_i^* v_i\rangle\rangle$, which is a key element in the modeling of two-phase flows. Figure 4 shows that, during the early times, the alignment decreases rapidly as the droplets are unable to adjust to fast evolution of the turbulence. At long times, however, the effects of the initial conditions are diminished, and the turbulence is more established so that it is easier for the droplets to follow the fluid motion. As expected, two-way coupling improves the alignment by modifying the velocity of the surrounding fluid to mimic some of the features of the droplet velocity. Because smaller droplets have less inertia and more easily follow the fluid motion, a larger alignment is observed for the case with $\tau_{d0} = 0.5\tau_{d0b}$. The change in the mass-loading ratio has very little effect on the alignment at long times. This is expected as the response of a droplet to changes in the flow primarily depends on its time constant.

In the stochastic modeling of two-phase flows, of great interest is the form of the probability density function (PDF) of the droplet velocity fluctuation. In Fig. 6 the temporal evolution of the skewness ($\langle\langle v_1^3\rangle\rangle / \langle\langle v_1^2\rangle\rangle^{3/2}$) and kurtosis ($\langle\langle v_1^4\rangle\rangle / \langle\langle v_1^2\rangle\rangle^2$) of the droplet fluctuating velocity in the streamwise direction are presented; similar trends were observed in other directions. The general observation is that the PDF of the droplet velocity is not significantly affected by evaporation and chemical reaction. The skewness is very close to zero throughout the simulation, and, except for a short time around $St = 3$, the kurtosis values remain close to three. These values are very similar to those for a normal distribution and suggest that the droplet velocity fluctuations can be accurately modeled by a Gaussian PDF. This is true in particular at long times when the turbulence and the droplets reach some quasiequilibrium states.

Figure 7a shows the temporal variations of the Reynolds average temperature of the carrier phase. A slight growth in the temperature is observed in the absence of a chemical reaction (i.e., for the one-way case) caused by the energy added to the system by the mean

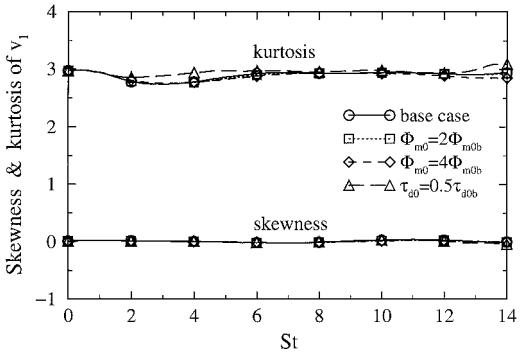

Fig. 6 Skewness and kurtosis of the droplet fluctuating velocity in the streamwise direction.

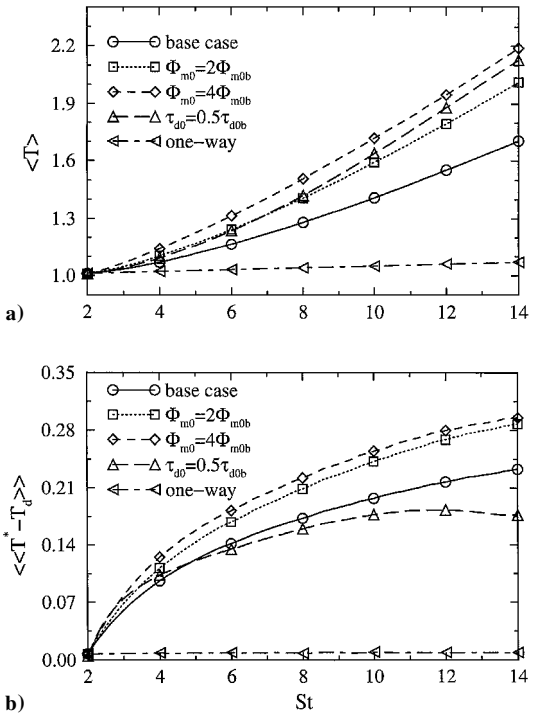

Fig. 7 Temporal variations of a) the mean carrier-phase temperature and b) the Lagrangian mean temperature difference.

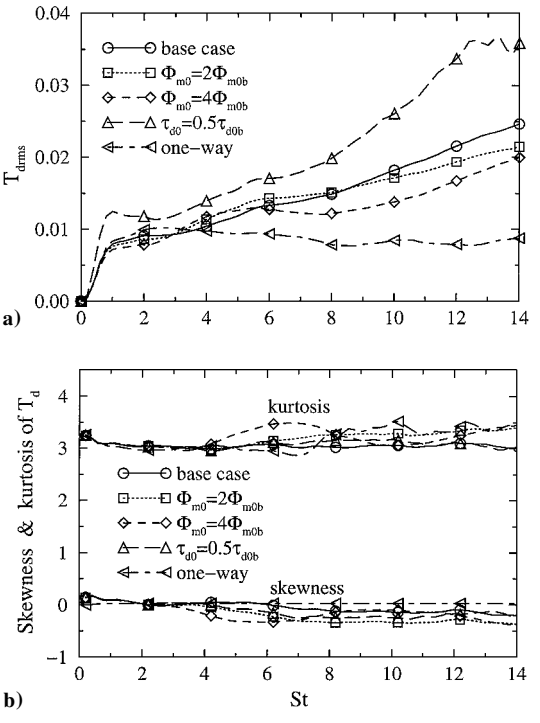

Fig. 8 Temporal variations of a) rms and b) skewness and kurtosis of the droplet temperature.

shear. As expected, the growth rate is much larger in the presence of chemical reaction. Part of the heat released by reaction is consumed for the latent heat of evaporation and does not contribute to the increase of the temperature. To investigate the heat transfer between the two phases, in Fig. 7b we demonstrate the temporal variation of the Lagrangian mean temperature difference, calculated based on the gas temperature at the droplet location T^*. This difference increases in time for all of the reacting cases. One exception is the case with $\tau_{d0} = 0.5\tau_{d0b}$ at long times caused by the full evaporation of a portion of the droplets as was discussed earlier in this section. The temperature difference at a long time is smaller for this case as compared to the base case, despite a higher mean temperature of the carrier phase, which is a result of the smaller heat capacity ($m_d C_p$) of the smaller droplets. The temperature of these droplets can be increased by a lower rate of convective heat transfer (i.e., a smaller temperature difference) as compared to larger droplets. Regarding the effects of the mass-loading ratio, we note that with the increase of this parameter the total amount of the vaporized fuel increases. This results in the increase of the total heat released by combustion, and larger values for $\langle T \rangle$ are attained. Under these circumstances the droplets can also receive more energy (by convection) from the carrier phase, as demonstrated by larger values of $\langle\langle T^* - T_d \rangle\rangle$.

The effects of evaporation and chemical reaction on the temperature fluctuation can be further studied by considering the temporal variation of the rms of this quantity. Figure 8a shows the variations of $T_{\text{drms}} = [\langle\langle (T_d - \langle\langle T_d \rangle\rangle)^2 \rangle\rangle]^{1/2}$ for the droplets. It is observed in Fig. 8a that, in the absence of the chemical reaction, the curve for the one-way coupling case approaches an asymptotic value at long times. The rms temperature for cases with chemical reaction, however, does not reach asymptotic values. Further analysis of the results indicated that the rms values are smaller for temperature fluctuations of the droplets than those of the fluid (not shown). This is mainly caused by the larger heat capacity of the droplets, which makes them more resistant to thermal disturbances. For the same reason the rms temperature is larger for the case with a smaller initial droplet time constant. The trend of variation of the rms temperature with the mass-loading ratio is not as clear, although it appears that at long times T_{drms} decreases with the increase of the mass-loading ratio. To investigate the effects of reaction on the PDF of the droplet temperature fluctuations, in Fig. 8b the temporal evolution of the skewness and kurtosis of T_d is shown. It appears that the skewness and kurtosis values for various cases are close to those for a Gaussian PDF and suggest that, in the absence of more accurate information, the PDF of the droplet temperature fluctuation can be approximated by a normal distribution. An interesting feature noted in Fig. 8b is that chemical reaction results in negative skewness, i.e., a larger number of the droplets exhibit temperatures lower than the mean temperature. This can be explained by considering the fact that, by generating smaller amounts of fuel vapor, the smaller droplets are associated with regions of the flow with smaller reaction rate. This is also verified by flow visualizations in Ref. 4, which indicate the

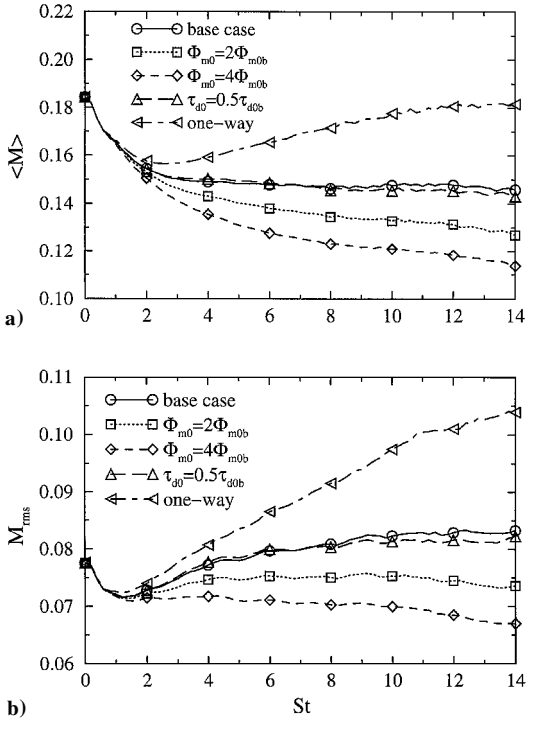

Fig. 9 Temporal variations of a) the mean and b) the rms of the turbulence Mach number.

presence of smaller droplets outside of the intense reaction zone toward the end of the simulations. These droplets receive less energy from the combustion and exhibit smaller temperatures, thus resulting in negative skewness factors for the droplet temperature.

The effects of the droplets on the turbulence Mach number $M = [u_i u_i/(\gamma RT)]^{1/2}$ are investigated by considering the temporal variations of the Reynolds average and the rms values of this quantity. A comparison with the one-way coupling case indicates that both the mean and the rms of the Mach number decrease in the presence of chemical reaction. This is in agreement with previous studies in single-phase flows in that the chemical reaction diminishes the compressibility effects.[21] The decrease of the Mach number is despite the fact that the velocity fluctuations may increase when the droplets are allowed to react (cf. Fig. 2b for $\tau_{d0} = 0.5\tau_{d0b}$). Figure 7a shows that the temperature of the carrier phase significantly increases for cases with chemical reaction. This results in the increase of the speed of sound and the decrease of the Mach number. The results in Fig. 9 also show that the Mach number is small for various cases and the carrier phase is free of shocklets. This is an important issue in this study as a Fourier pseudospectral method has been used for the simulation of the carrier phase.

Conclusion

Results of numerical simulations are used to investigate the effects of the mass-loading ratio and the droplet time constant on statistics of temperature and velocity in a reacting droplet-laden homogeneous shear turbulence. The chemical reaction takes place in the carrier phase and is described by a single-step, second-order irreversible scheme. The homogeneous flow considered here can be viewed as one of the basic flows locally dominating in a more general flow of practical interest. As a result, the statistics presented here can be used for a preliminary assessment of statistical/stochastic models for two-phase turbulent flows. The results of the simulations are primarily used to investigate the effects of the droplet time constant and the mass-loading ratio. The decrease of the droplet time constant (or the droplet size) significantly modifies the behavior of both phases, which is caused mainly by the increase of the evaporation rate, which in turn results in higher heat release by combustion. Further, the decrease of the droplet time constant results in the enhancement of both the turbulence kinetic energy and its viscous dissipation rate, while increasing the alignment between the fluctuating velocities of the two phases. The influence of the mass-loading ratio is primarily a result of the two-way coupling effects that tend to modify the behavior of the carrier phase to mimic some of the main features of the dispersed phase. This decreases the turbulence kinetic energy of the carrier phase by introducing the extra dissipation caused by drag. The alignment of the particle and fluid fluctuating velocities, however, is not influenced by the increase of the mass-loading ratio, which shows that the alignment is primarily a function of the droplet time constant that determines the response of the particle to local changes in the flow. Both the mean temperature of the carrier phase and the Lagrangian mean temperature difference (between the two phases) increase with the increase of the mass-loading ratio. The rms of the droplet temperature fluctuations increases in time in the presence of chemical reaction and shows an increase with the decrease of the droplet time constant. The results suggest that the droplet velocity and temperature fluctuations can be reasonably approximated with Gaussian distribution; this is more strongly true for velocity fluctuations.

Acknowledgments

The support for this work was provided by the U.S. Office of Naval Research under Grant N00014-99-1-0808 with G. D. Roy as Technical Monitor and by the National Science Foundation under Grant CTS-9874655 with M. C. Roco as Program Director. Computational resources were provided by the San Diego Supercomputing Center.

References

[1] Simonin, O., Deutsch, E., and Boivin, M., "Large Eddy Simulation and Second-Moment Closure Model of Particle Fluctuating Motion in Two-Phase Turbulent Shear Flows," *Turbulent Shear Flows*, Vol. 9, edited by F. Durst, N. Kasagi, B. Launder, F. Schmidt, and J. Whitelaw, Springer-Verlag, New York, 1995, pp. 85–115.

[2] Taulbee, D. B., Mashayek, F., and Barré, C., "Simulation and Reynolds Stress Modeling of Particle-Laden Turbulent Shear Flows," *International Journal of Heat Fluid Flow*, Vol. 20, No. 4, 1999, pp. 368–373.

[3] Hyland, K. E., McKee, S., and Reeks, M. W., "Exact Analytic Solutions to Turbulent Particle Flow Equations," *Physics of Fluids*, Vol. 11, No. 5, 1999, pp. 1249–1261.

[4] Mashayek, F., "Numerical Investigation of Reacting Droplets in Homogeneous Shear Turbulence," *Journal of Fluid Mechanics*, Vol. 405, 2000, pp. 1–36.

[5] Wang, L.-P., and Maxey, M. R., "Settling Velocity and Concentration Distribution of Heavy Particles in Isotropic Turbulence," *Journal of Fluid Mechanics*, Vol. 256, 1993, pp. 27–68.

[6] Eaton, J. K., and Fessler, J. R., "Preferential Concentration of Particles by Turbulence," *International Journal of Multiphase Flow Supplement*, Vol. 20, Supplementary Issue, 1994, pp. 169–209.

[7] Riley, J. J., and Patterson, G. S., "Diffusion Experiments with Numerically Integrated Isotropic Turbulence," *Physics of Fluids*, Vol. 17, No. 2, 1974, pp. 292–297.

[8] Squires, K. D., and Eaton, J. K., "Particle Response and Turbulence Modification in Isotropic Turbulence," *Physics of Fluids*, Vol. 2, No. 7, 1990, pp. 1191–1203.

[9] Elghobashi, S., and Truesdell, G. C., "On the Two-Way Interaction Between Homogeneous Turbulence and Dispersed Solid Particles. I: Turbulence Modification," *Physics of Fluids*, Vol. 5, No. 7, 1993, pp. 1790–1801.

[10] Mashayek, F., Taulbee, D. B., and Givi, P., "Modeling and Simulation of Two-Phase Turbulent Flow," *Propulsion Combustion: Fuels to Emissions*, edited by G. D. Roy, Taylor and Francis, Washington, DC, 1998, pp. 241–280, Chap. 8.

[11] Mashayek, F., "Droplet-Turbulence Interactions in Low-Mach-Number Homogeneous Shear Two-Phase Flows," *Journal of Fluid Mechanics*, Vol. 376, 1998, pp. 163–203.

[12] Mashayek, F., Barré, C., and Taulbee, D. B., "Direct Numerical Simulation of Particle-Laden Homogeneous Plain Strain Turbulent Flow," *The Proceedings of the First International Symposium on Turbulence and Shear Flow Phenomena*, edited by S. Banerjee and J. K. Eaton, Begell House, Inc., New York, 1999, pp. 115–120.

[13] McLaughlin, J. B., "Aerosol Particle Deposition in Numerically Simulated Channel Flow," *Physics of Fluids*, Vol. 1, No. 7, 1989, pp. 1211–1224.

[14] Samimy, M., and Lele, S. K., "Motion of Particles with Inertia in a Compressible Free Shear Layer," *Physics of Fluids*, Vol. 3, No. 8, 1991, pp. 1915–1923.

[15] Pan, Y., and Banerjee, S., "Numerical Simulation of Particle Interactions with Wall Turbulence," *Physics of Fluids*, Vol. 8, No. 10, 1996, pp. 2733–2755.

[16] Miller, R. S., and Bellan, J., "Direct Numerical Simulation of a Confined Three-Dimensional Gas Mixing Layer with One Evaporating Hydrocarbon-Droplet Laden Stream," *Journal of Fluid Mechanics*, Vol. 384, 1999, pp. 293–338.

[17] Turns, S. R., *An Introduction to Combustion: Concepts and Applications*, McGraw–Hill, New York, 1996, pp. 195–199.

[18] Crowe, C. T., Sharma, M. P., and Stock, D. E., "The Particle-Source in Cell (PSI-Cell) Model for Gas-Droplet Flows," *Journal of Fluids Engineering*, Vol. 6, June 1977, pp. 325–332.

[19] Liljegren, L. M., "The Effect of a Mean Fluid Velocity Gradient on the Streamwise Velocity Variance of a Particle Suspended in a Turbulent Flow," *International Journal of Multiphase Flow*, Vol. 19, No. 3, 1993, pp. 471–484.

[20] Reeks, M. W., "On the Constitutive Relations for Dispersed Particles in Nonuniform Flows. I: Dispersion in a Simple Shear Flow," *Physics of Fluids*, Vol. 5, No. 3, 1993, pp. 750–761.

[21] Jaberi, F. A., and Madnia, C. K., "Effects of Heat of Reaction on Homogeneous Compressible Turbulence," *Journal of Scientific Computing*, Vol. 13, No. 2, 1998, pp. 201–228.